Soft Matter

PAPER

Check for updates

Osmotic forces modify lipid membrane fluctuations

Amaresh Sahu (iD)

In hydrodynamic descriptions of lipid bilayers, the membrane is often approximated as being impermeable to the surrounding, solute-containing fluid. However, biological and *in vitro* lipid membranes are influenced by their permeability and the resultant osmotic forces—whose effects remain poorly understood. Here, we study the dynamics of a fluctuating, planar lipid membrane that is ideally selective: fluid can pass through it, while solutes cannot. We find that the canonical membrane relaxation mode, in which internal membrane forces are balanced by fluid drag, no longer exists over all wavenumbers. Rather, this mode only exists when it is slower than solute diffusion—corresponding to a finite range of wavenumbers. The well-known equipartition result, quantifying the size of membrane undulations due to thermal perturbations, is consequently limited in its validity to the aforementioned range. Moreover, this range shrinks as the membrane surface tension is increased, and above a critical tension, the membrane mode vanishes. Our findings are relevant when interpreting experimental measurements of membrane fluctuations, especially in vesicles at moderate to high tensions.

Introduction

Biological membranes are unique materials that surround the cell and compartmentalize its internal organelles. While such membranes are slowly permeable to water,[1] large neutral molecules (such as sugars) cannot easily pass through them.[2] The semipermeability of lipid membranes is relevant to both biological and *in vitro* scenarios—as in both cases, membranes are essentially always surrounded by solutes. While the general equations governing the coupled membrane, fluid, and solute dynamics were recently obtained,[3] there is not yet a systematic characterization of membrane behavior. As a result, the effects of permeability and osmosis on lipid membrane dynamics remain poorly understood.

The present study investigates how planar lipid membranes act on, and are influenced by, their surrounding environment. Flat membranes are found in various biological settings, including the endoplasmic reticulum,[4] Golgi complex,[5] and neuromuscular junction.[6] In addition, theories of impermeable bilayer fluctuations about a flat surface are often used to describe the thermal undulations of giant unilamellar vesicles (GUVs). We begin by investigating an impermeable membrane, where the dynamics of the solute are not considered. By starting with a well-understood system (see, *e.g.*, ref. 7–19), we are better equipped to study our primary system of interest: the semipermeable membrane. The temporal evolution of the

normal modes is determined for the linearized dynamics, and the relative time scale of membrane and solute relaxation is found to govern the nature of the coupled dynamics. When solutes relax more quickly, the dynamics are indistinguishable from the impermeable scenario. It is then straightforward to present an effective Langevin equation including thermal perturbations, and obtain the magnitude of the resultant height fluctuations. In contrast, when the membrane relaxes more quickly than the surrounding solutes, the resultant dynamics are qualitatively different from their impermeable counterpart. As a result, the character of thermal undulations—long assumed to be that of an impermeable membrane when analyzing fluctuating GUVs—is no longer known. Experimental consequences of our findings are highlighted, and avenues for future work are discussed.

The impermeable membrane

Consider a nearly planar lipid membrane surrounded by water. For the present analysis, we neglect solutes and make the standard approximation that the membrane is impermeable to fluid. Water is characterized by its three-dimensional mass density ρ_f, shear viscosity μ_f, and kinematic viscosity $\nu_f := \mu_f/\rho_f$. Relevant membrane parameters are the patch length ℓ_c, two-dimensional (2D) areal density ρ_m, surface tension λ_c, and bending modulus k_b.[20] It is important to note that surface tension is not a membrane property, but rather takes the requisite value to enforce areal incompressibility.[21,22] As a

McKetta Department of Chemical Engineering, University of Texas, Austin, TX, 78712, USA. E-mail: asahu@che.utexas.edu

Table 1 Membrane, fluid, and solute parameters

Parameter	Sym.	Value	Ref.
Patch size	ℓ_c	10^2–10^3 nm	4 and 6
Density	ρ_m	10^{-8} pg nm^{-2}	28
Bending modulus	k_b	10^2 pN nm	29
Surface tension	λ_c	10^{-4}–10^{-1} pN nm^{-1}	29,30
Impermeability	κ	10^3–10^5 pN μs nm^{-3}	1,31
Density	ρ_f	10^{-9} pg nm^{-3}	—
Shear viscosity	μ_f	10^{-3} pN μs nm^{-2}	—
Kinematic viscosity	ν_f	10^6 nm^2 μs^{-1}	—
Concentration	c_0	10^{-1} nm^{-3}	32
Diffusivity	D	10^3 nm^2 μs^{-1}	33

result, the membrane surface tension can span a wide range of values and is often tuned in experiments.[23,24] Characteristic values of all parameters are provided in Table 1.

Our base state is an unperturbed membrane sheet lying in the x–y plane, surrounded on both sides by a semi-infinite stationary fluid. We seek to understand how the coupled membrane and fluid system responds to small perturbations. To this end, we determine the linearized dynamics of the coupled membrane and fluid system about the base configuration. In what follows, an abbreviated analysis of the governing equations is presented; see Section S2 of the SI[25] for further details.

The governing equations

The position $\boldsymbol{x}$ of the perturbed membrane is given by $\boldsymbol{x}(x,y,t) = x\boldsymbol{e}_x + y\boldsymbol{e}_y + h(x,y,t)\boldsymbol{e}_z$, where $x,y \in [0,\ell_c]$ and $|h| \ll \ell_c$ by construction. For planar geometries with a stationary base state, the in-plane and out-of-plane membrane equations are decoupled.[26,27] To solve for the time evolution of the membrane height in the absence of thermal fluctuations, we require only the z-component of the linear momentum balance of the membrane—often called the shape equation and given by[27]

$$\rho_m h_{,tt} = \lambda_c h_{,\alpha\alpha} - \frac{k_b}{2} h_{,\alpha\alpha\beta\beta} - [\![p]\!]. \tag{1}$$

In eqn (1), $\alpha,\beta \in 1,2$ denote directions in the x–y plane, with repeated indices summed over such that (for example) $h_{,\alpha\alpha} = h_{,xx} + h_{,yy}$. Here, $(\cdot)_{,t} := \partial(\cdot)/\partial t$ is the partial time derivative and $[\![p]\!] := p^+ - p^-$ is the difference in the fluid pressure above (+) and below (−) the membrane. The pressure and velocity fields, $p^\pm$ and $v_j^\pm$ (where Roman indices span $\{1,2,3\}$ and repeated indices are summed over), satisfy the incompressible Navier–Stokes equations linearized about the base state: $v_{j,j}^\pm = 0$ and $\rho_f v_{j,t}^\pm = \mu_f v_{j,kk}^\pm - p_{,j}^\pm$. With the no-slip boundary condition $h_{,t} = v_z^\pm$ at the membrane surface, water cannot flow through the membrane and we have a well-posed set of equations for the coupled system (ref. 25, Section 2).

At this point, we follow standard approaches to solve for the dynamics of the system. The membrane height is decomposed into planar Fourier modes as

$$h(x,y,t) = \sum_q \hat{h}_q e^{i(q_x x + q_y y)} e^{-\omega_q t}, \tag{2}$$

where the wavevector $\boldsymbol{q} = (q_x,q_y)$ has corresponding wavenumber $q := (q_x^2 + q_y^2)^{1/2} \sim 10^{-4}$–$10^{-1}$ nm^{-1}, ω_q is the associated relaxation frequency, and normal modes are assumed to be independent. Fluid unknowns are similarly decomposed into planar Fourier modes, with the functional dependence on z to be solved for. The fluid pressure, for example, is expressed as

$$p^\pm(x,y,z,t) = \sum_q \hat{p}_q^\pm(z) e^{i(q_x x + q_y y)} e^{-\omega_q t}. \tag{3}$$

Our main task is to solve for all frequencies ω_q satisfying the governing equations. In doing so, we also solve for the pressure and velocity fields in the fluid.

The frequency solutions

As we limit ourselves to the linearized dynamics, all unknowns of a particular wavevector q are proportional to the membrane height $\hat{h}_q$. We assume $\hat{h}_q \neq 0$ and combine all equations governing the membrane and fluid into a single equation for ω_q, namely, the dispersion relation (see Section S2.3 of the SI[25]). Given the physically motivated requirement that all fluid perturbations decay far from the membrane surface, there are two frequencies at each wavenumber, which are plotted in Fig. 1. The aforementioned equation for ω_q is not straightforward to interpret—though we find that the dynamics are well-approximated by

$$\rho_{eff}\omega_q^2 - 4\mu_f q\omega_q + E = 0. \tag{4}$$

Eqn (4), with the temporal ansatz $h \sim e^{-\omega t}$ in eqn (2), shows that the dynamics of the membrane are analogous to that of the spring–mass–damper from introductory mechanics. Here, $\rho_{eff} := \rho_m + 4\rho_f/q \sim 10^{-7}$–$10^{-5}$ pg nm^{-2} approximates the combined inertia of the membrane and fluid, $4\mu_f q \sim 10^{-7}$–10^{-4} pN μs nm^{-3} is the well-known hydrodynamic drag from the surrounding fluid, and $E := \lambda_c q^2 + \frac{1}{2} k_b q^4 \sim 10^{-12}$–$10^{-2}$ pN nm^{-3} captures the energetics of small membrane fluctuations: $\frac{1}{2}\ell_c^2 E|\hat{h}_q^2|$
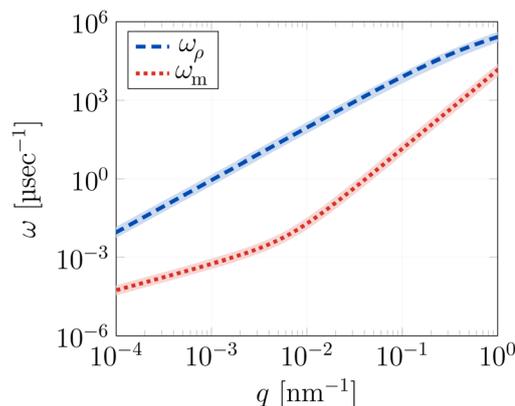

Fig. 1 Plot of the two impermeable frequency solutions as a function of wavenumber. Blue dashed and red dotted lines are the exact inertial and membrane branches, respectively, obtained numerically. The approximate solutions in eqn (5) are shown as thick, transparent bands. Relevant parameters are $\rho_f = 10^{-9}$ pg nm^{-3}, $\nu_f = 9 \times 10^{-5}$ nm^2 μs^{-1}, $\rho_m = 10^{-8}$ pg nm^{-2}, $\lambda_c = 2 \times 10^{-3}$ pN nm^{-1}, and $k_b = 10^2$ pN nm.

is the energy of mode q to quadratic order.[34] As the system is overdamped, $4\mu_{\mathrm{f}}q \gg \sqrt{\rho_{\mathrm{eff}}E}$ and the two solutions to eqn (4) are well-approximated by

$$\tilde{\omega}_\rho := \frac{4\mu_{\mathrm{f}}q}{\rho_{\mathrm{eff}}} \quad \text{and} \quad \tilde{\omega}_{\mathrm{m}} := \frac{E}{4\mu_{\mathrm{f}}q}. \tag{5}$$

In eqn (5), the 'tilde' accent indicates that eqn (4) is only an approximation of the true dynamics; the subscripts ρ and m designate the inertial and membrane branches. As shown in Fig. 1, the frequencies in eqn (5) are a good approximation to the true solution.

The membrane response. Following eqn (4) and (5), let us denote the two exact frequency branches as ω_ρ and ω_{m}. The membrane height, in real space, is then given by [*cf.* eqn (2)]

$$h(x, y, t) = \sum_q \left(\hat{h}_q^\rho \mathrm{e}^{-\omega_\rho t} + \hat{h}_q^{\mathrm{m}} \mathrm{e}^{-\omega_{\mathrm{m}} t} \right) \mathrm{e}^{i(q_x x + q_y y)}, \tag{6}$$

where $\hat{h}_q^\rho$ and $\hat{h}_q^{\mathrm{m}}$ are determined upon specification of the initial conditions: h and $\partial h/\partial t$ at time $t = 0$. Since $\omega_\rho \gg \omega_{\mathrm{m}}$ over all wavenumbers, the inertial branch quickly decays and the dynamics of the coupled system are captured by the membrane branch. Prior studies are accordingly justified in neglecting inertial effects throughout their investigations of planar lipid membrane behavior.[7–19,35–39]

The fluid response. To understand the dynamics of the fluid as the membrane relaxes, consider two disturbances to a specific mode q. In the first case, $\hat{h}_q^{\mathrm{m}} = 0$ and only the inertial mode is excited, while in the second case, $\hat{h}_q^\rho = 0$ and only the membrane mode is excited [see eqn (6)]. In both cases, the pressure field (3) is given by $\hat{p}_q^\pm = \mp\frac{1}{2}(\rho_{\mathrm{m}}\omega_q^2 + E)\hat{h}_q \mathrm{e}^{-q|z|}$. The magnitude of the pressure at $z = 0$ is determined using eqn (1), and the decay length $1/q$ is a consequence of the pressure field being harmonic: $p_{,jj}^\pm = 0$. In contrast, fluid velocities decay over the two length scales $1/q$ and $1/k_\nu$, where $k_\nu := (q^2 - \omega/\nu_{\mathrm{f}})^{1/2}$ is a modified wavenumber that accounts for the inertia of the fluid (see Section S94 of ref. 40 and Section S2.1 of the SI[25]). As a consequence of the time scale separation $\omega_\rho \gg \omega_{\mathrm{m}}$, $1/\bar{q} \approx 1/k_\nu$ on the membrane branch and $1/\bar{q} \ll 1/k_\nu$ on the inertial branch.

The semipermeable membrane

With an understanding of the impermeable membrane, we are primed to investigate the primary system of interest: a semipermeable membrane, in which fluid flows through the membrane, while solutes dissolved in the fluid do not. Solutes are characterized by a base concentration $c_0 \sim 0.1$ nm^{-3} (ref. 32) and a diffusion constant $D \sim 10^3$ nm^2 μs^{-1}.[33] In addition, the membrane impermeability κ relates the flux of water through the bilayer to its driving force;[3] here, $\kappa \sim 10^3$–10^5 pN μs nm^{-3}.[1,31] Dynamical effects from water permeation are of order $\mu_{\mathrm{f}}q/\kappa$: a dimensionless parameter that we call the permeability number $\mathcal{P}$, ranging from 10^{-7} to 10^{-12} over wavenumbers $q \in (10^{-4}, 10^{-1})$ nm^{-1}. We will show $\mathcal{P} \to 0$ in the limit of an impermeable membrane; lipid bilayers are thus nearly impermeable.

The governing equations

The membrane shape equation (1) remains unchanged in the presence of solutes.[3] The perturbed concentrations $c^\pm$ above and below the membrane, with $|c^\pm| \ll c_0$, evolve according to the diffusion equation $c_{,t}^\pm = Dc_{,jj}^\pm$. Solute impermeability is enforced by requiring the total solute flux through the membrane—comprising diffusive and convective contributions—to be zero:

$$-Dc_{,z}^\pm + c_0 \left(v_z^\pm - h_{,t} \right) = 0. \tag{7}$$

In eqn (7), velocities and concentration gradients are evaluated at the membrane surface. The equation governing water permeation through an arbitrarily curved and deforming lipid membrane was recently obtained by A. M. Alkadri and K. K. Mandadapu,[3] who extended several seminal findings.[41–43] These authors used techniques from irreversible thermodynamics and differential geometry to show that fluid flow through the membrane is driven by differences in hydrodynamic tractions and osmotic pressures across the membrane surface. For nearly planar geometries and an ideally selective membrane, the findings from ref. 3 simplify to

$$\kappa(v_z^\pm - h_{,t}) = k_{\mathrm{B}}\vartheta[\![c]\!] - [\![p]\!], \tag{8}$$

where k_{B} is Boltzmann's constant, ϑ is the absolute temperature, and $[\![c]\!] := c^+ - c^-$ is the jump in solute concentration at the membrane surface. In the language of irreversible thermodynamics,[44,45] eqn (8) presents a linear relationship between the thermodynamic driving force ($k_{\mathrm{B}}\vartheta[\![c]\!] - [\![p]\!]$) and the corresponding thermodynamic flux ($v_z^\pm - h_{,t}$), with the latter being a measure of fluid flow through the membrane. The phenomenological parameter κ, understood as a transport coefficient,[3] captures the resistance to flow: for a given driving force, a larger value of κ corresponds to a smaller water flux through the membrane. Eqn (8) is equivalently expressed as $v_z^\pm - h_{,t} = (k_{\mathrm{B}}\vartheta[\![c]\!] - [\![p]\!])/\kappa$; in the limit of $\kappa \to \infty$ or $\mathcal{P} \to 0$ we find $v_z^\pm \to h_{,t}$ and recover the impermeable scenario.

The diffusive time scale. The presence of solutes in the surrounding fluid introduces a diffusive frequency

$$\tilde{\omega}_D := q^2 D. \tag{9}$$

Fig. 2a shows $\tilde{\omega}_D$ plotted on top of the curves in Fig. 1; note that the diffusive and impermeable membrane frequencies can be comparable. Let us denote $q_0^\pm$ as the two wavenumbers at which the diffusive and membrane time scales are equal. From eqn (5) and (9), we find

$$q_0^\pm = \frac{4\mu_{\mathrm{f}}D}{k_{\mathrm{b}}}\left[1 \pm \left(1 - \frac{\lambda_{\mathrm{c}}k_{\mathrm{b}}}{8\mu_{\mathrm{f}}^2 D^2}\right)^{1/2}\right], \tag{10}$$

with $\tilde{\omega}_{\mathrm{m}} < \tilde{\omega}_D$ when $q \in (q_0^-, q_0^+)$, and $\tilde{\omega}_{\mathrm{m}} > \tilde{\omega}_D$ otherwise. Since the base surface tension $\lambda_{\mathrm{c}} \sim 10^{-4}$–$10^{-1}$ pN nm^{-1} is not a material parameter, but rather varies—and can be tuned—across systems, $q_0^\pm$ is plotted at different tensions λ_{c} in Fig. 2b to reveal a dome-like envelope. There exists a critical

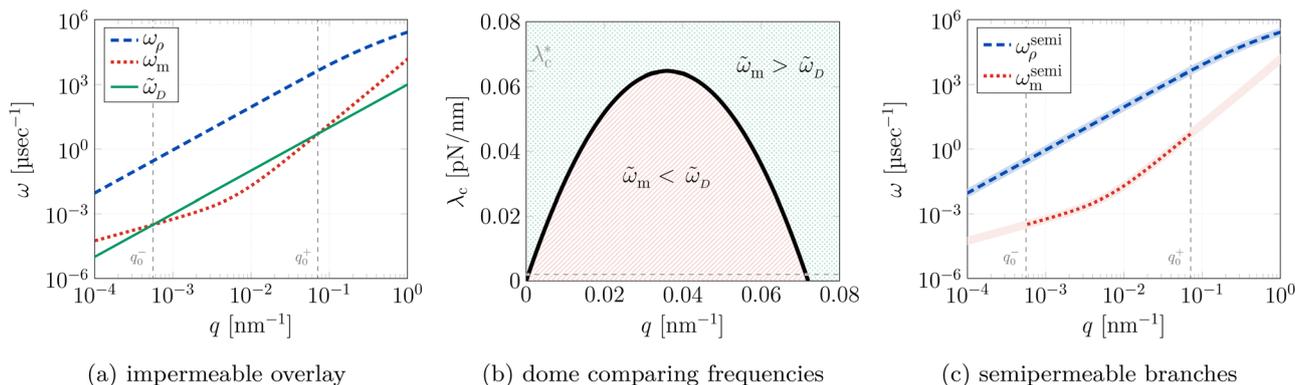(a) impermeable overlay   (b) dome comparing frequencies   (c) semipermeable branches

Fig. 2 Relevance of the diffusive time scale to the dynamics of the semipermeable system. (a) An overlay of $\tilde{\omega}_D$ (solid green line) on top of the impermeable frequencies in Fig. 1. There are two wavenumbers for which the impermeable membrane frequency ω_m^{imp} equals $\tilde{\omega}_D$; approximating the former as $\tilde{\omega}_m$ yields the two crossover wavenumbers q_0^- and q_0^+ (10)—shown as vertical, dashed lines. (b) Plot of $q_0^\pm$ over a range of the base membrane tension λ_c, which varies across systems. The surface tension from (a) of $\lambda_c = 2 \times 10^{-3}$ pN nm^{-1} is shown as the horizontal dashed line. There exists a critical tension λ_c^* (11) above which $\tilde{\omega}_m > \tilde{\omega}_D$ for all wavenumbers. (c) Plot of the real parts of the semipermeable frequencies (dotted or dashed solid lines), overlaid on top of the impermeable frequencies (thick, transparent bands) for comparison. The inertial branch is essentially unchanged. The membrane branch only exists when $\omega_m < \tilde{\omega}_D$ and is thus confined to the range $q \in (q_0^-, q_0^+)$. For base membrane tensions $\lambda_c > \lambda_c^*$, the membrane branch vanishes altogether.

base tension

$$\lambda_c^* := \frac{8\mu_f^2 D^2}{k_b} \sim 6 \times 10^{-2} \text{ pN nm}^{-1} \qquad (11)$$

at the top of the dome, above which no real q_0 exists. We also note that the bilayer tears at the lysis tension $\lambda_\ell \sim 1$–10 pN nm^{-1}.[1] Thus, when the base membrane tension λ_c lies between λ_c^* and λ_ℓ, we have $\tilde{\omega}_m > \tilde{\omega}_D$ over all wavenumbers. As we will see, the relative values of $\tilde{\omega}_m$ and $\tilde{\omega}_D$—and thus whether a mode is "inside" (*i.e.* below) or "outside" (*i.e.* above) the dome in Fig. 2b—govern different regimes of membrane behavior.

The frequency solutions. Membrane and fluid unknowns are expressed as in the impermeable analysis, with the concentration expanded in planar normal modes as [*cf.* eqn (3)]

$$c^\pm(x, y, z, t) = \sum_q \hat{c}_q^\pm(z) e^{i(q_x x + q_y y)} e^{-\omega_q t}. \qquad (12)$$

In our linearized description, all perturbed bulk quantities are again proportional to the membrane height. Assuming a nontrivial solution ($\hat{h}_q \neq 0$), it is straightforward to arrive at the dispersion relation, as shown in Section S3.3 of the SI.[25] While ω_q cannot be solved for analytically, we take advantage of the smallness of $\mathcal{P}$: since the membrane is nearly impermeable, semipermeable frequencies are close to their impermeable counterparts. In what follows, we investigate how the dynamics of the impermeable branches are altered by the presence of solutes in the surrounding medium.

The inertial branch. We begin by assuming that concentration modes evolve with the impermeable inertial frequency ω_ρ^{imp}, such that for a single mode, $c_{,t}^\pm = -\omega_\rho^{imp} c^\pm$ (see eqn (12)). As a consequence, the diffusion equation $c_{,t}^\pm = D c_{,ii}^\pm$ for the mode q simplifies to $-\omega_\rho^{imp} \hat{c}_q^\pm = D(-q^2 \hat{c}_q^\pm + \mathrm{d}^2 \hat{c}_q^\pm / \mathrm{d}z^2)$—which after

some rearrangement yields

$$\frac{\mathrm{d}^2 \hat{c}_q^\pm}{\mathrm{d}z^2} = -q^2 \tilde{\eta}^2 \hat{c}_q^\pm. \quad \text{Here} \quad \tilde{\eta} := \left(\frac{\omega_\rho^{imp}}{\tilde{\omega}_D} - 1\right)^{1/2} \qquad (13)$$

is a positive, real, dimensionless parameter defined for notational convenience. Eqn (13) admits the two purely oscillatory solutions $\hat{c}_q^+ \sim e^{\pm iq\tilde{\eta}z}$. As these standing waves do not decay as $z \to \infty$, we seek the lowest-order concentration correction due to the semipermeability of the membrane.[†]

We first recognize that water permeation alters the hydrodynamic drag on the membrane by the surrounding fluid. Eqn (7) and (8) together yield $[\![p]\!] = k_B \vartheta [\![c]\!] - (\kappa D/c_0) c_{,z}^\pm$, which—along with eqn (1)—shows that standing waves in the concentration add a hydrodynamic drag force $90°$ out of phase with the membrane velocity. We show in the SI (ref. 25, Section 3.2) that an approximate dispersion relation for the semipermeable membrane is given by [*cf.* eqn (4)]

$$\rho_{eff} \omega_q^2 - 4\mu_f q \omega_q + E = \pm \frac{8i \mathcal{P}\mathcal{S}}{\tilde{\eta}}(4\mu_f q)\omega_q. \qquad (14)$$

In eqn (14), $\mathcal{S} := k_B \vartheta c_0/(D\kappa q) \sim 10^{-8} - 10^{-3} \ll 1$ is a dimensionless parameter that arises when eqn (7) and (8) are combined. The solution of eqn (14) closest to ω_ρ^{imp}, to lowest order in the product $\mathcal{P}\mathcal{S}$ of small parameters, is given by

$$\omega_\rho \approx \omega_\rho^{imp}(1 \pm 8i\mathcal{P}\mathcal{S}/\tilde{\eta}). \qquad (15)$$

Membrane permeability and osmotic forces accordingly introduce exceedingly slow temporal oscillations to the inertial dynamics of the coupled system.

The modification to the inertial frequency in eqn (15) also alters the spatial concentration of the solutes. Substituting eqn (15) into the diffusion equation and solving for the

---

† For conciseness, only the concentration field above the membrane is presented; see the SI (ref. 25, Sections 3.2 and 3.3) for all details.

concentration field yield

$$\hat{c}_{\boldsymbol{q}}^{+} \sim \exp\left\{\pm iq\tilde{\eta}z - \frac{4\mathcal{PS}qz}{1 - \tilde{\omega}_D/\omega_\rho^{\mathrm{imp}}}\right\}. \qquad (16)$$

Importantly, $\hat{c}_{\boldsymbol{q}}^{+} \to 0$ as $z \to \infty$ and concentration perturbations due to the fluctuating membrane decay far from the membrane surface. We have thus found a physically meaningful solution for both the frequency (15) and concentration (16) over all wavenumbers. The validity of our approximate analysis is confirmed in Fig. 2c: the impermeable branch is visually indistinguishable from the real portion of its semipermeable counterpart.

The membrane branch when diffusion is slow. As in the analysis of the inertial branch, we start by assuming that the solute concentration evolves at the frequency of the impermeable system—in this case, the membrane frequency $\omega_{\mathrm{m}}^{\mathrm{imp}}$. For wavenumbers $q \notin (q_0^-, q_0^+)$, diffusion is slow relative to the membrane and $\omega_{\mathrm{m}}^{\mathrm{imp}} > \tilde{\omega}_D$. The solute diffusion equation once again simplifies to eqn (13), where now $\tilde{\eta}$ involves $\omega_{\mathrm{m}}^{\mathrm{imp}}$ instead of $\omega_\rho^{\mathrm{imp}}$. With this change, and following a similar analysis to that described in the inertial scenario, we once again arrive at eqn (14). The membrane frequency is then found to be given by

$$\omega_{\mathrm{m}} \approx \omega_{\mathrm{m}}^{\mathrm{imp}}(1 \mp 8i\mathcal{PS}/\tilde{\eta}). \qquad (17)$$

Importantly, the sign of the imaginary part of ω_{m} is opposite to that of ω_ρ [*cf.* eqn (15)], and the out-of-phase drag force alters the inertial and membrane dynamics in different ways. Substituting eqn (17) into the diffusion equation gives the concentration field [*cf.* eqn (16)],

$$\hat{c}_{\boldsymbol{q}}^{+} \sim \exp\left\{\pm iq\tilde{\eta}z + \frac{4\mathcal{PS}qz}{1 - \tilde{\omega}_D/\omega_{\mathrm{m}}^{\mathrm{imp}}}\right\}. \qquad (18)$$

The concentration field in eqn (18) diverges as $z \to \infty$ and is not physically meaningful. As a consequence, the membrane branch vanishes when $q \notin (q_0^-, q_0^+)$. A representative result at low tension is shown in Fig. 2(c), and at tensions larger than λ_{c}^* (11), the membrane branch vanishes entirely.

The membrane branch when diffusion is fast. When $\omega_{\mathrm{m}}^{\mathrm{imp}} < \tilde{\omega}_D$ and $q \in (q_0^-, q_0^+)$, the analysis of the coupled system is straightforward in the limit of small $\mathcal{P}$. The diffusion equation, assuming $\omega = \omega_{\mathrm{m}}^{\mathrm{imp}}$ at lowest order, simplifies to $\mathrm{d}^2\hat{c}_{\boldsymbol{q}}^{\pm}/\mathrm{d}z^2 = (q^2 - \omega_{\mathrm{m}}^{\mathrm{imp}}/D)\hat{c}_{\boldsymbol{q}}^{\pm}$. We thus find the exponentially decaying concentration solutions

$$\hat{c}_{\boldsymbol{q}}^{\pm} \sim \exp\left\{\mp qz\left(1 - \frac{\omega_{\mathrm{m}}^{\mathrm{imp}}}{\tilde{\omega}_D}\right)^{1/2}\right\}. \qquad (19)$$

With no oscillations in the lowest-order concentration field, modifications to the hydrodynamic drag felt by the membrane are in phase with the membrane velocity. Moreover, as such corrections are of order $\mathcal{P} \ll 1$, we expect the membrane branch to be indistinguishable from its impermeable counterpart—as confirmed in Fig. 2(c).

Theoretical implications. As mentioned previously, solutes are present in the fluid surrounding nearly all artificial and biological membranes. Our findings demonstrate that such systems can only be approximated as impermeable for wavenumbers "inside the dome," where $q \in (q_0^-, q_0^+)$ and there is a slow frequency $\omega \approx E/(4\mu_{\mathrm{f}}q)$. In contrast, only a quickly decaying inertial mode exists for wavenumbers $q \notin (q_0^-, q_0^+)$ "outside the dome." For this case, (i) the membrane response is independent of k_{b} and λ_{c} at linear order and (ii) thermal perturbations (discussed subsequently) drive membrane undulations to continuously grow until saturated by nonlinear forces—both of which are surprising results.

The predictions described above motivate us to question whether our normal mode ansatz is indeed appropriate outside the dome. Here, we examine this issue from a statistical mechanical perspective. By starting with a microscopic Hamiltonian of the lipid, water, and solute molecules, one can integrate over fast degrees of freedom to obtain a free energy functional that depends only on the concentration field and membrane height.[46] When solutes are fast relative to the membrane, concentration degrees of freedom can also be integrated over to yield a free energy which depends only on the membrane height. We thus recover a description similar to that of the impermeable scenario. If instead solutes are slow relative to the membrane, the concentration field is not equilibrated for a given, instantaneous bilayer shape. Upon integrating over the slow solute degrees of freedom, the resultant membrane equation inerits this slowness *via* a memory kernel—for which the time evolution of the membrane depends on its history, and there is no associated free energy functional or equipartition result.[47] While such a result is incompatible with our normal mode ansatz, it justifies the membrane behaving qualitatively differently inside and outside the dome. Further analysis, likely involving nonlinear simulations of the membrane and surrounding fluid,[48–54] is required to understand the dynamics of the coupled system. In any case, however, we emphasize that the standard impermeable result is not applicable for wavenumbers outside the dome.

Experimentally characterizing GUVs

In experimental investigations of lipid bilayers, one often seeks to characterize membrane material properties prior to further manipulation. When GUVs are involved, their fluctuations from thermal disturbances can be imaged and—with a theory of membrane undulations—processed to determine k_{b} and λ_{c}.[29,31,55–61] While most experimental investigations apply the well-understood impermeable theory over all wavenumbers, the present study reveals that only modes inside the dome should be treated as impermeable. Moreover, as the behavior of undulations outside the dome is not currently well-understood, experimental measurements involving these modes should be excluded when determining membrane properties. In what follows, we discuss how to incorporate thermal perturbations into our theory and then analyze GUV fluctuation data from experiments.

The impermeable Langevin equation. When the lipid bilayer is treated as impermeable, its linear response to perturbations is well-known. Since inertial modes decay much more quickly than their membrane counterparts (see eqn (6) with $\omega_\rho \gg \omega_m$), inertia can be neglected entirely; the membrane frequency $\tilde{\omega}_m$ presented in eqn (5) is then exact. Decomposing the membrane height as $h(x, y, t) = \sum_q \tilde{h}_q(t) e^{i(q_x x + q_y y)}$ leads to the Langevin equation [cf. eqn (2) and (4)]

$$\frac{d\tilde{h}_q}{dt} + \tilde{\omega}_m \tilde{h}_q = \tilde{\xi}_q(t). \tag{20}$$

In eqn (20), $\tilde{\xi}_q(t)$ is a complex Gaussian thermal noise satisfying the fluctuation–dissipation theorem, with two-time correlations proportional to $\delta(t - t') k_B \vartheta/(4\mu_f q \ell_c^2)$.[18] Eqn (20) can be solved exactly to yield[62]

$$\left\langle |\tilde{h}_q|^2 \right\rangle = \frac{k_B \vartheta}{E \ell_c^2}, \tag{21}$$

which is the well-known result of the equipartition theorem as applied to planar membranes.[34]

The Langevin equation inside the dome. For modes with $q \in (q_0^-, q_0^+)$, there is no discernible difference between the impermeable and semipermeable dynamics. Thus, eqn (20) once again applies, and membrane fluctuations satisfy the equipartition result (21).

The Langevin equation outside the dome. As discussed previously, we are currently unsure if our normal mode ansatz is appropriate outside the dome. If the ansatz is indeed valid, then we effectively see only an inertial mode. The corresponding Langevin equation describing membrane fluctuations is given by

$$\frac{1}{\omega_\rho^{(r)}} \frac{d^2\tilde{h}_q}{dt^2} + \frac{d\tilde{h}_q}{dt} = \tilde{\xi}_q(t), \tag{22}$$

where $\omega_\rho^{(r)}$ is the real part of the frequency and $\tilde{\xi}_q$ is the same thermal noise as in eqn (20). There is no elastic restoring force in eqn (22), which is analogous to the equation of motion for a colloidal particle in a fluid. Just as a colloid diffuses freely at long times,[62] the variance of membrane height undulations grows linearly in time according to eqn (22). Eventually, the membrane height will grow to a point where our assumption of linearity is no longer valid. At this point, membrane bending and surface tension forces will presumably prevent height fluctuations from continuing to grow—yet a description of such behavior is beyond the scope of the present work. Thus, irrespective of whether our ansatz is valid, membrane
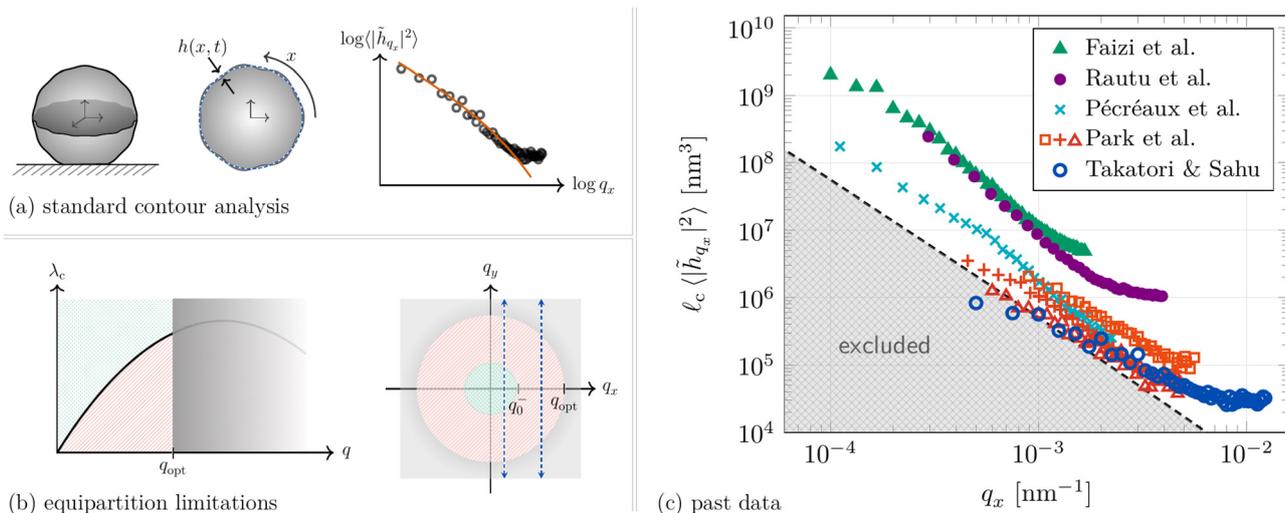

Fig. 3 Analysis of GUV contour fluctuations, modified due to membrane semipermeability. (a) Canonical protocol to calculate the bending modulus and surface tension of a fluctuating GUV. In a spherical vesicle of radius r_v (left), the equatorial cross-section is imaged (center) at successive time intervals. Radial deviations from a circle are recorded as $h(x,t)$, where x is the arclength along the unperturbed circle. The shape disturbances $h(x,t)$ are decomposed into one-dimensional Fourier modes, whose thermally averaged amplitudes (right; adapted from ref. 55) are fit to eqn (23) by tuning the values of k_b and λ_c (right; solid orange line).[29] Theory and experiment deviate at large q_x due to finite optical resolution in the latter. (b) Limitations of the equipartition result (21) due to solutes in the surrounding fluid. (left) Modes inside the dome (red lines) satisfy eqn (21); those outside the dome (green dots) do not. Membrane undulations cannot be visualized above $q_{opt} \approx 0.025$ nm^{-1} (gray shading) due to limitations in the optical resolution.[31] (right) For a GUV with surface tension $\lambda_c \in (0, \lambda_c^*)$, modes are characterized in the q_x–q_y plane. The equipartition result (21) is limited to modes with amplitude $q > q_0^-$, and large-q modes cannot be visualized. The domains of integration in eqn (23), corresponding to two different values of q_x, are shown as dashed vertical lines. The result of eqn (23) is invalid when $q_x < q_0^-$, as in such cases, the integral contains modes outside the dome. (c) Plot of experimental membrane fluctuations, over a range of reported surface tensions λ_c, from prior studies: the studies by Faizi et al.[59] (3.1×10^{-6} pN nm^{-1}), Rautu et al.[58] (1.4×10^{-5} pN nm^{-1}), Pécréaux et al.[29] (1.7×10^{-4} pN nm^{-1}), Park et al.[57] (7×10^{-4}–3×10^{-3} pN nm^{-1}), and Takatori and Sahu[55] (4×10^{-3} pN nm^{-1}). The y-axis is chosen to be independent of the vesicle radius and depends only on λ_c and k_b [see eqn (23)]. At large q_x, the data saturate due to optical resolution limitations. All data points below the dashed black line are outside the dome and should be excluded when determining membrane parameters. Fluctuation data from the high-tension vesicle in ref. 56 are not publicly available, and so cannot be plotted—though the first 88 modes should be excluded based on the reported value of $\lambda_c = 0.025$ pN nm^{-1} (ref. 25, Section 4).

fluctuations are not expected to satisfy the equipartition result outside the dome where $q \notin (q_0^-, q_0^+)$.

The standard contour analysis of a GUV. Fig. 3(a) shows the canonical analysis of a GUV undergoing thermal fluctuations, the details of which can be found in ref. 29. In short, the equatorial cross-section of a GUV is imaged at frequent time intervals. For each snapshot, the radial deviation from a circle of radius r_v is measured and decomposed into normal modes. As GUVs are large and weakly curved, it is often convenient to apply the planar membrane theory[29]—which is simpler than its spherical counterpart.[31,58–60] The position x is defined as the distance along the circle, with $h(x,t)$ being the radial perturbation, $\ell_c = 2\pi r_v$, and $q_x = 2\pi m/\ell_c = m/r_v$ for positive integers m. The one-dimensional (1D) fluctuation spectrum $\langle |\tilde{h}_{q_x}|^2 \rangle$ is calculated from experimental measurements, as shown in Fig. 3(a). To compare the 1D data with the theoretical 2D equipartition result of eqn (21), the latter is averaged over all q_y as[29]

$$\begin{aligned} \left\langle |\tilde{h}_{q_x}|^2 \right\rangle &= \frac{\ell_c}{2\pi} \int_{-\infty}^{\infty} \mathrm{d}q_y \left\langle |\tilde{h}_q|^2 \right\rangle \\ &= \frac{k_B \vartheta}{2\lambda_c \ell_c} \left(\frac{1}{q_x} - \frac{1}{\sqrt{q_x^2 + 2\lambda_c/k_b}} \right). \end{aligned} \tag{23}$$

The bending modulus k_b and surface tension λ_c are chosen so as to minimize the difference between the measured fluctuation spectrum and prediction of eqn (23)—which, in Fig. 3(a), are shown as black circles and an orange line, respectively. Note that short-wavelength fluctuations cannot be visualized in experiments due to a lower bound $\ell_{opt} \approx 250$ nm on the optical resolution, which sets an upper limit $q_{opt} := 2\pi/\ell_{opt} \approx 0.025$ nm^{-1} beyond which undulations cannot be observed.[31] In practice, short-wavelength modes are excluded when fitting k_b and λ_c. Techniques also exist to correct for the finite camera integration time[29] and vertical focal projections,[58] but are not discussed here.

The modified contour analysis of a GUV. When solutes are present in the fluid surrounding the membrane, the 2D equipartition result (21) is only valid for modes q with magnitude $|q| \in (q_0^-, q_0^+)$. We seek to determine how the experimental analysis of contour fluctuations is altered by such a restriction. To this end, we first note that $q_{opt} < q_0^+$, as shown in Fig. 3(b). Short-wavelength undulations outside the dome thus cannot be observed in experiments and do not contribute to the determination of k_b and λ_c. Long-wavelength fluctuations outside the dome, on the other hand, are captured experimentally. Fig. 3(b) characterizes modes in the q_x–q_y plane as being either outside the dome ($|q| < q_0^-$), inside the dome and visually accessible ($q_0^- < |q| < q_{opt}$), or visually inaccessible ($|q| > q_{opt}$). Here, domains of the contour integral in eqn (23) for two values of q_x are shown as dashed vertical lines. If $q_x < q_0^-$, this domain contains modes for which the equipartition result (21) does not apply. The result of eqn (23), which relies on eqn (21), is accordingly valid only when $q_x > q_0^-$—with the understanding that as q_x increases, fewer modes are optically accessible.

To determine k_b and λ_c from GUV contour fluctuations, it is useful to plot fluctuation amplitudes as shown in Fig. 3(c)—which contains experimental data from several prior investigations.[29,55,57–59] Here, both the x-axis and y-axis are chosen to be independent of r_v [$cf.$ eqn (23)]. Next, experimental data inside and outside the dome need to be identified. To this end, we combine eqn (10) and (23) to obtain the fluctuation amplitudes of 1D modes $q_x = q_0^-$ on the dome, for tensions $\lambda_c \in (0, \lambda_c^*)$:

$$\ell_c \left\langle |\tilde{h}_{q_x}|^2 \right\rangle = \frac{k_B \vartheta \left(1 - \sqrt{k_b q_x/(8\mu_f D)}\right)}{q_x^2 (8\mu_f D - k_b q_x)}. \tag{24}$$

Importantly, k_b is not known a priori, and so eqn (24) can be approximated as $\ell_c \langle |\tilde{h}_{q_x}|^2 \rangle \approx k_B \vartheta/(8\mu_f q_x^2 D)$—valid when $k_b q_x \ll 8\mu_f D$—in a first analysis of the data. Eqn (24) is plotted as the dashed black line in Fig. 3(c); all of the data points below it are outside the dome and should be excluded when determining k_b and λ_c.

Our aggregation and analysis of the experimental data in Fig. 3(c) are detailed in Section S4 of the SI.[25] Most often, vesicle tensions $\lambda_c \sim 10^{-7}$–10^{-4} pN nm^{-1} are low[29,58–60] and all data lie inside the dome. As it turns out, a vesicle at low tension is experimentally favorable because its undulations are large and hence easy to image. In many cases, the vesicle's osmotic environment is manipulated to elicit a low tension. Notable exceptions are the so-called active vesicles containing either self-propelled Janus particles or motile bacteria.[55–57] For these systems, moderate vesicle tensions are required for active particles to not overcome the elastic membrane restoring force and form a tube. Given the fluctuation data for active vesicles in Fig. 1 of ref. 55 and Fig. 6(c) of ref. 57, between one and eight long-wavelength modes lie outside the dome (ref. 25, Section 4)—though the overall findings of these studies are unaffected. In contrast, for the high-tension ($\lambda_c = 0.025$ pN nm^{-1}) active vesicle in Fig. 1(g) of ref. 56, the first 88 long-wavelength modes lie outside the dome. It is likely that upon excluding these modes, the calculated values of k_b and λ_c would be affected. Unfortunately, the experimental fluctuation data for this vesicle are not provided, and we cannot investigate further. Nevertheless, we find that osmotic forces can indeed alter membrane fluctuations in biologically relevant scenarios.

Concluding remarks

In this work, we investigated the linearized dynamics of a planar lipid membrane, surrounded by a Newtonian fluid in which solutes are dissolved. Though the lipid bilayer is only weakly permeable to water, the presence of solutes can significantly alter its dynamics. More specifically, when $\tilde{\omega}_D < \tilde{\omega}_m$ and diffusion is slow relative to the impermeable membrane, undulations of the semipermeable system no longer decay at a frequency near $\tilde{\omega}_m$. In such cases, either (i) the ansatz that all quantities can be expressed in terms of planar normal modes as in eqn (2), (3), and (12) is no longer valid or (ii) the bilayer only decays at the fast inertial frequency $\omega_\rho \gg \omega_m$. When thermal

perturbations are incorporated into the theory, the well-known equipartition result (21) is found to only be experimentally relevant when $q \in (q_0^-, q_{opt})$—a range that narrows as λ_c is increased. Our results are relevant when membrane tensions are large, as is the case with active vesicles[55–57] and a variety of biological scenarios.[30,63–74]

The vanishing of the membrane mode at low q and large λ_c opens several lines of inquiry. We are particularly interested to see if membranes in spherical or cylindrical geometries respond in the same fashion; the former is needed for a careful analysis of GUV undulations,[58–60] while the latter could be relevant to neuronal systems.[30,63–66] In all scenarios where the membrane branch vanishes, the behavior of the coupled membrane–fluid–solute system can be interrogated with non-linear simulations.[48–54] Additional levels of complexity can be introduced by considering membranes that are not ideally selective,[3] have a finite thickness,[75–78] or are surrounded by charged solutes—with the latter requiring extensive theoretical developments.[76–80]

Conflicts of interest

There are no conflicts to declare.

Data availability

The code used to generate all data in the present study is publicly available at https://github.com/sahu-lab/osmosis-flat.

Supplementary information (SI): theoretical techniques used and methods of numerical solution.[25] See DOI: https://doi.org/10.1039/d5sm01094b.

Acknowledgements

References

1 K. Olbrich, W. Rawicz, D. Needham and E. Evans, *Biophys. J.*, 2000, **79**, 321–327.

2 R. E. Wood, F. P. Wirth Jr and H. E. Morgan, *Biochim. Biophys. Acta*, 1968, **163**, 171–178.

3 A. M. Alkadri and K. K. Mandadapu, *Phys. Rev. E*, 2025, **112**, 034413.

4 M. Terasaki, *et al.*, *Cell*, 2013, **154**, 285–296.

5 K. Tanaka and H. Fukudome, *J. Elec. Microsc. Tech.*, 1991, **17**, 15–23.

6 S. Watanabe, *et al.*, *eLife*, 2013, **2**, e00723.

7 J. Prost and R. Bruinsma, *Europhys. Lett.*, 1996, **33**, 321.

8 R. Granek, *J. Phys. II France*, 1997, **7**, 1761–1788.

9 F. L. H. Brown, *Biophys. J.*, 2003, **84**, 842–853.

10 H.-Y. Chen, *Phys. Rev. Lett.*, 2004, **92**, 168101.

11 N. S. Gov, *Phys. Rev. Lett.*, 2004, **93**, 268104.

12 L. C.-L. Lin and F. L. H. Brown, *Phys. Rev. Lett.*, 2004, **93**, 256001.

13 D. Lacoste and A. W. C. Lau, *Europhys. Lett.*, 2005, **70**, 418.

14 M. A. Lomholt, *Phys. Rev. E: Stat., Nonlinear, Soft Matter Phys.*, 2006, **73**, 061914.

15 E. Ben-Isaac, *et al.*, *Phys. Rev. Lett.*, 2011, **106**, 238103.

16 B. Loubet, U. Seifert and M. A. Lomholt, *Phys. Rev. E: Stat., Nonlinear, Soft Matter Phys.*, 2012, **85**, 031913.

17 R. Alert, J. Casademunt, J. Brugués and P. Sens, *Biophys. J.*, 2015, **108**, 1878–1886.

18 K. Sapp and L. Maibaum, *Phys. Rev. E*, 2016, **94**, 052414–052423.

19 H. Turlier and T. Betz, Fluctuations in active membranes, in *Physics of Biological Membranes*, ed. P. Bassereau and P. Sens, Springer, Cham, 2018, pp. 581–619.

20 Some studies define kb/2 as the bending modulus.

21 D. J. Steigmann, *Arch. Ration. Mech. Anal.*, 1999, **150**, 127–152.

22 A. Sahu, Irreversible Thermodynamics and Hydrodynamics of Biological Membranes, PhD thesis, University of California at Berkeley, 2022.

23 R. S. Gracià, N. Bezlyepkina, R. L. Knorr, R. Lipowsky and R. Dimova, *ASoft Matter*, 2010, **6**, 1472–1482.

24 Y. A. Ayala, R. Omidvar, W. Römer and A. Rohrbach, *Nat. Commun.*, 2023, **14**, 65.

25 See the SI, where the governing equations are presented and dispersion relations are obtained. Methods of numerical solution are described, and all associated codes are present in the repository github.com/sahu-lab/osmosis-flat.

26 A. Sahu, R. A. Sauer and K. K. Mandadapu, *Phys. Rev. E*, 2017, **96**, 042409.

27 A. Sahu, A. Glisman, J. Tchoufag and K. K. Mandadapu, *Phys. Rev. E*, 2020, **101**, 052401 .

28 P. Parkkila, M. Elderdfi, A. Bunker and T. Viitala, *Langmuir*, 2018, **34**, 8081–8091.

29 J. Pécréaux, H.-G. Döbereiner, J. Prost, J.-F. Joanny and P. Bassereau, *Eur. Phys. J. E*, 2004, **13**, 277–290.

30 J. Dai, M. P. Sheetz, X. Wan and C. E. Morris, *J. Neurosci.*, 1998, **18**, 6681–6692.

31 J. H. Ipsen, A. G. Hansen and T. Bhatia, Vesicle fluctuation analysis, in *The Giant Vesicle Book*, ed. R. Dimova and C. Marques, CRC Press, Boca Raton, 1st edn, 2020, pp. 333–345.

32 R. Dimova, *et al.*, *J. Phys.: Condens. Matter*, 2006, **18**, S1151–S1176.

33 L. J. Gosting and M. S. Morris, *J. Am. Chem. Soc.*, 1949, **71**, 1998–2006.

34 F. Brochard and J. F. Lennon, *J. Phys.*, 1975, **36**, 1035–1047.

35 B. A. Camley and F. L. H. Brown, *Phys. Rev. Lett.*, 2010, **105**, 148102.

36 N. Oppenheimer and H. Diamant, *Biophys. J.*, 2009, **96**, 3041–3049.

37 H. A. Stone and H. Masoud, *J. Fluid Mech.*, 2015, **781**, 494–505.

38 B. A. Camley, M. G. Lerner, R. W. Pastor and F. L. H. Brown, *J. Chem. Phys*, 2015, **143**, 243113.

39 V. C. Suja, N. Oppenheimer and H. A. Stone, *Phys. Rev. Fluids*, 2025, **10**, L041101.

40 S. Chandrasekhar, *Hydrodynamic and Hydromagnetic Stability*, Dover, New York, 1981.

41 E. H. Starling, *J. Physiol.*, 1896, **19**, 312–326.

42 A. J. Staverman, *Recl. Trav. Chim. Pays-Bas*, 1951, **70**, 344–352.

43 O. O. Kedem and A. Katchalsky, *Biochim. Biophys. Acta*, 1958, **27**, 229–246.

44 I. Prigogine, *Introduction to Thermodynamics of Irreversible Processes*, Interscience Publishers, 1961.

45 S. R. de Groot and P. Mazur. *Non-Equilibrium Thermodynamics*, Dover, 1984.

46 D. T. Limmer, *Statistical Mechanics and Stochastic Thermodynamics: A Textbook on Modern Approaches in and out of Equilibrium*, Oxford University Press, 2024.

47 R. W. Zwanzig, *Nonequilibrium Statistical Mechanics*, Oxford University Press, New York, 2001.

48 V. Narsimhan, A. P. Spann and E. S. G. Shaqfeh, *J. Fluid Mech.*, 2015, **777**, 1–26.

49 A. Torres-Sánchez, D. Millán and M. Arroyo, *J. Fluid Mech.*, 2019, **872**, 218–271.

50 D. A. Rower, M. Padidar and P. J. Atzberger, *J. Comp. Phys.*, 2022, **455**, 110994.

51 P. D. Tran, T. A. Blanpied and P. J. Atzberger, *Phys. Rev. E*, 2022, **106**, 044402.

52 A. Torres-Sánchez, M. K. Winter and G. Salbreux, *PLOS Comput. Biol.*, 2022, **18**, e1010762.

53 A. Sahu, *J. Fluid Mech.*, 2025, **1020**, A46.

54 D. Wörthmüller, G. Ferraro, P. Sens and M. Castellana, *arXiv*, 2025, preprint, arXiv:2506.17827, DOI: 10.48550/arXiv.2506.17827.

55 S. C. Takatori and A. Sahu, *Phys. Rev. Lett.*, 2020, **124**, 158102.

56 H. R. Vutukuri, *et al.*, *Nature*, 2020, **586**, 52–56.

57 M. Park, K. Lee and S. Granick, *Soft Matter*, 2022, **18**, 6419–6425.

58 S. A. Rautu, *et al.*, *Soft Matter*, 2017, **13**, 3480–3483.

59 H. A. Faizi, C. J. Reeves, V. N. Georgiev, P. M. Vlahovska and R. Dimova, *Soft Matter*, 2020, **16**, 8996–9001.

60 H. A. Faizi, R. Granek and P. M. Vlahovska, *Proc. Natl. Acad. Sci. U. S. A.*, 2024, **121**, e2413557121.

61 K. Lee, G. Chommanov, H.-S. Jang and S. Granick, *J. Phys. Chem. A*, 2020, **124**, 4512–4516.

62 S. Chandrasekhar, *Rev. Mod. Phys.*, 1943, **15**, 1–89.

63 J. Dai and M. P. Sheetz, *Biophys. J.*, 1995, **68**, 988–996.

64 A. Datar, *et al.*, *Biophys. J.*, 2019, **117**, 880–891.

65 P. A. Pullarkat, P. Dommersnes, P. Fernández, J.-F. Joanny and A. Ott, *Phys. Rev. Lett.*, 2006, **96**, 048104.

66 J. Tchoufag, A. Sahu and K. K. Mandadapu, *Phys. Rev. Lett.*, 2022, **128**, 068101.

67 R. E. Goldstein, P. Nelson, T. Powers and U. Seifert, *J. Phys. II*, 1996, **6**, 767–796.

68 T. R. Powers and R. E. Goldstein, *Phys. Rev. Lett.*, 1997, **78**, 2555–2558.

69 S. Boulant, C. Kural, J.-C. Zeeh, F. Ubelmann and T. Kirchhausen, *Nat. Cell. Biol.*, 2011, **13**, 1124–1131.

70 S. C. Al-Izzi, G. Rowlands, P. Sens and M. S. Turner, *Phys. Rev. Lett.*, 2018, **120**, 138102.

71 Z. Shi, Z. T. Graber, T. Baumgart, H. A. Stone and A. E. Cohen, *Cell*, 2018, **175**, 1769–1779.

72 S. C. Al-Izzi, M. S. Turner and P. Sens, *arXiv*, 2024, preprint, arXiv:2409.14835, DOI: 10.48550/arXiv.2409.14835.

73 M. Janssen, S. Liese, S. C. Al-Izzi and A. Carlson, *Phys. Rev. E*, 2024, **109**, 044403.

74 A. Venkatesh, A. Bhargava and V. Narsimhan, *J. Fluid Mech.*, 2025, **1003**, A18.

75 Z. G. Lipel, Y. A. D. Omar and D. Fraggedakis, *Phys. Rev. Fluids*, 2025, **10**, 103101.

76 Y. A. D. Omar, Z. G. Lipel and K. K. Mandadapu, *Phys. Rev. E*, 2024, **109**, 054401.

77 Y. A. D. Omar, Z. G. Lipel and K. K. Mandadapu, *Phys. Rev. E*, 2025, **112**, 024406.

78 Y. A. D. Omar, Z. G. Lipel and K. K. Mandadapu, *Phys. Rev. E*, 2025, **112**, 024407.

79 K. D. Fong, H. K. Bergstrom, B. D. McCloskey and K. K. Mandadapu, *AIChE J.*, 2020, **66**, e17091.

80 Z. Yu, S. Zhao, M. J. Miksis and P. M. Vlahovska, *Phys. Rev. E*, 2025, **112**, 054408.